

Urothermal Syntheses of Chiral Zinc Benzotriazole-5-carboxylate Frameworks for Iodine Uptake^①

HUANG Zai-Chun^a WANG Xiao-Fang^a GOHI Bi Foua Claude Alain^{a②}

LI Yu-Feng^a KANG Yao^{b②} JIANG Zhi-Qiang^{a②}

^a (Deep-processing of Fine Flake Graphite Sichuan Province Key Laboratory of Colleges and Universities, Panzhihua University, Panzhihua 617000, China)

^b (State Key Laboratory of Structural Chemistry, Fujian Institute of Research on the Structure of Matter, Chinese Academy of Sciences, Fuzhou 350002, China)

ABSTRACT So far, the synthesis of chiral framework with achiral organic ligand still faces great challenge. Herein, three new coordinated complexes [Zn(btca)Cl] DMA N(CH₃)₂ (**1**), [Zn(btca)(Ac[−])] N(CH₃)₂ (**2**) and [Zn(btca)] H₂O (**3**) (DMA = N,N-dimethylacetamide, btca = benzotriazole-5-carboxylate acid) were synthesized via different methods. Single-crystal X-ray diffraction analysis revealed that compounds **1** and **2** were isostructural and showed achiral layer network with **fes** topology, and **3** presented a chiral three-dimensional framework with **eta** topology. The result of this work has demonstrated that urothermal synthesis will be promising means of constructing chiral framework with achiral building block. Compound **3** also displayed an excellent property of iodine uptake.

Keywords: urothermal synthesis, benzotriazole-5-carboxylate acid, chirality, I₂ absorption;

DOI: 10.14102/j.cnki.0254-5861.2011-2796

1 INTRODUCTION

During the past several decades, crystalline metal-organic frameworks (MOFs) had received intensive attention due to their specific properties, as well as intriguing structures, in which inorganic component and organic linker are assembled together by strong coordination bond and regularly arranged in designated location in the lattice^[1-5]. But up to now, a lot of efforts are still devoted to synthesize this new crystalline material due to several potential applications in many highly active fields, such as gas storage/separation, small/large molecule absorption, fluorescence sensor, drug delivery and catalysis^[6-19]. Although both metal units and organic components can play a crucial role in the unique shape and prospective function, the structural evolution and stability of framework can be also affected by solvents or synthesis method. The different combination of solvents and their dosage proportion are usually used as effective strategy to

demonstrate the structural evolution^[20-25], which can be further explained by one of Li's recent works^[26]. In this reported work, a series of intriguing multicomponent trinuclear copper pyrazolate metal-organic frameworks were assembled by combining N,N-dimethylformamide (DMF), N,N-dimethylacetamide (DMA) and N-methyl-2-pyrrolidone (NMP). In addition to focusing on the solvent, choosing suitable synthetic method is also useful to various architectures based on similar metal units and organic linkers^[27, 28]. In 2010, Zhang and Bu developed a new synthetic method, named urothermal synthesis^[29]. During this synthetic process, urea derivatives have competed with homologues or other solvents like DMF or DEF to coordinate to metal sites, which can be utilized to control the structure of framework.

As a subclass of MOFs, crystalline chiral MOFs, especially homochiral MOF materials, have received explosive attention, owing to their potential applications in enantioselective processes, heterogeneous asymmetric catalysis and sensor

Received 5 March 2020; accepted 12 May 2020 (CCDC 1988086-1988088)

① This project was supported by the Science and Technology Planning Project in Sichuan Province (2019YJ0686), the Science and Technology Planning Project in Panzhihua City (2019ZD-G-11)

② Corresponding authors. Gohi Bi Foua Claude Alain, Ph.D, E-mail: claudefouabi@hotmail.fr;

Kang Yao, Ph.D, professor, E-mail: ky@fjirsm.ac.cn; Jiang Zhi-Qiang, Ph.D, professor, E-mail: myjiangzq@163.com

technology in optoelectronics^[30-35]. However, such chiral MOFs can generally be constructed from chiral organic ligands, and only a limited number of chiral MOFs were synthesized by achiral organic linker^[36-39]. After being inspired by the strategy that N-donor ligand and O-donor ligands could be simultaneously employed to extend structure and functionality, many aromatic organic ligands containing carboxylic and nitrogen donor groups, such as imidazoledicarboxylic and triazoledicarboxylic acids, have been researched extensively in constructing a series of metal-organic materials^[40-43]. However, it is rare to use above-mentioned achiral carboxylic and nitrogen donor ligand to fabricate chiral frameworks, which suggests that the preparation of chiral framework with this kind of organic ligand is still faced with a great challenge because many uncertain problems originating from versatile linker factors and variable metallic coordination configuration have yet to be overcome. Despite the fact that it still plays an essential role in the field of biosciences, functional materials and so on, iodine also has certain drawbacks, such as radioactive ¹²⁹I, which is a source of severe environmental pollution. Iodine uptake is therefore important to counter its harmful effects on the environment. As far as we know, it is very rare that chiral MOFs were employed to absorb iodine.

In this work, we used benzotriazole-5-carboxylate acid as a multidentate organic ligand to assemble chiral MOFs. In fact, merely a handful of framework with this ligand can be achieved, let alone chiral backbone, which may be modified through a new synthetic method. Herein, three complexes, namely [Zn(btca)Cl]·DMA·N(CH₃)₂ (**1**), [Zn(btca)(Ac⁻)]·N(CH₃)₂ (**2**) and [Zn(btca)]·H₂O (**3**), were obtained. It was interesting to note that their structures demonstrated the characteristic of structural diversities based on similar coordination mode in which **1** and **2** showed two-dimensional (2D) achiral network with **fes** topology, while **3** presented a three-dimensional chiral porous framework with **eta** topology. This meaningful result could be assigned to the urothermal synthesis with ethyleneurea (e-urea) and 1,3-dimethyl-3,4,5,6-tetrahydro-2(1H)-pyrimidinone (DMPU) as template agents. Meanwhile, compound **3** exhibited an excellent property of iodine uptake.

2 EXPERIMENTAL

2.1 Materials and measurements

All reagents and solvents were of analytic grade and were

purchased from Chinese commercial sources and used without further purification. Diffraction data were collected by using Saturn724+CCD and XCalibur E CCD diffractometers, respectively. The powder diffraction data were collected on a MiniFlex2 X-ray diffractometer.

2.2 Synthetic method

2.2.1 Syntheses of compounds **1** and **2**

ZnCl₂ (0.1207 g, 0.89 mmol) for **1**, Zn(NO₃)₂·6H₂O (0.1810 g, 0.63 mmol) for **2**, benzotriazole-5-carboxylate acid (btca, 0.0862 g, 0.49 mmol), pyrazine (0.0301 g, 0.38 mmol) and N,N-dimethylacetamide (DMA, 2 mL) were spilled into a 20 mL vial and stirred for 10 minutes. The mixture was kept into the oven at 130 °C for five days. Colorless transparent block-like crystals **1** were obtained. Compound **2** was synthesized similar to **1** with adding additional solvents of methanol (2 mL), acetonitrile (2 mL) and water (2 mL).

2.2.2 Synthesis of compound **3**

Compound **3** was synthesized by urothermal synthesis. Urothermal reaction of Zn(NO₃)₂·6H₂O (0.1807 g, 0.63 mmol), benzotriazole-5-carboxylate acid (btca, 0.0859 g, 0.48 mmol), pyrazine (0.0300 g, 0.38 mmol), e-urea (1.2 g) and DMPU (3 mL) in a 20 mL vial at 130 °C for 3 days produced colorless crystals and then cooled to room temperature. After washing with alcohol, the resulting compound **3** was obtained.

2.2.3 X-ray crystallography

Single-crystal X-ray diffraction data collection was performed on the computer-controlled Saturn 724+CCD diffractometer and XCalibur E CCD single-crystal diffractometer with graphite-monochromatic MoK α (λ = 0.71073 Å) at T = 293(2) K, respectively. The structure was solved by direct methods and refined by full-matrix least-squares methods on F^2 by using the SHELX-97 program package. All non-hydrogen atoms were refined anisotropically. Hydrogen atoms were generated geometrically. The crystallographic data, and related bond lengths and bond angles for compounds **1**~**3** are listed in Tables 1 and 2.

3 RESULTS AND DISCUSSION

3.1 Description of the crystal structure

Single-crystal X-ray diffractions of complexes **1** and **2** clarify that both of them crystallize in the same orthorhombic space group *Pbca*, which are isostructural frameworks. In their asymmetric units, there are only one independent metal center and one btca ligand. Zn(1) shows a distorted ZnN₂OCl (in compound **1**) or ZnN₂O₂ (in compound **2**) tetrahedral

geometry with two nitrogen atoms, originating from triazole rings, one oxygen atom from a monodentate carboxylate of btca ligand, a Cl^- for **1** and deprotonated acetic acid for **2** coordinated with a terminal site (Fig. 1a and 1c). The coordination mode of btca ligand in **1** and **2** is $\mu_3\text{-}\eta^1:\eta^0:\eta^1:\eta^0:\eta^1$. For the interactions between metal sites and ligands described above, two basic units are formed: every two Zn centers and two linkers form a $[\text{Zn}_2(\text{btca})_2]$ unit possessing a 14-membered ring; every four Zn centers and four linkers form a $[\text{Zn}_4(\text{btca})_4]$ unit with a 24-membered ring. The neighboring rings are arranged in an $\cdots\text{ABAB}\cdots$ order along a wavy curve along the c axis because both **1** and **2** exhibit overall wave-like layers (Fig. 1b and 1d). It is notable that the coordinated acetic acid molecules in complex **2** are arranged in “up” and “down” order along the c axis distributing on both sides of the layer. The layers in structures of **1** and **2** can be reduced as a 3-connected uninodal net (denoted: **fes**) with the point symbol of $\{4\ 8^2\}$ by reducing each btca organic linker and metal center as a 3-connected node, respectively (Fig. 1e).

In order to extend the structure of btca framework, two urea derivatives e-urea and DMPU were employed to induce structural evolution from achiral layer to chiral three-

dimensional network. Single-crystal X-ray diffraction of complex **3** reveals that it crystallizes in the trigonal space group $P3_221$. In the structure of **3**, the asymmetric unit still consisted of a single independent zinc center, one btca ligand and one solvent water molecule (Fig. 2a). As the same as in **1** and **2**, Zn atom in **3** also shows a distorted ZnN_2O_2 tetrahedral geometry with two nitrogen atoms originating from triazole rings, two oxygen atoms from one monodentate carboxylate of btca ligand and a terminal water molecule. Interestingly, due to the involvement of urea derivatives in the reaction, the coordination angle and geometric configuration of inorganic metal ion and organic linker are quite different from those of **1** and **2**, which resulted in the helical sub-structure **3**. As shown in Fig. 2b, both P - and M -helices can be observed in the porous framework. To clarify, the P - and M -helices are unseparated and uneven. These helical sub-structures in **3** intertwine to result in a three-dimensional chiral framework (Fig. 2c). From the viewpoint of topology, the resulting network can be also reduced as a 3-connected uninodal net (denoted: **eta**) with the point symbol of $\{8^3\}$ by considering both btca ligand and Zn center as a 3-connected node (Fig. 2d).

Table 1. Crystal Data and Structure Refinement for Complexes 1~3

Complex	1	2	3
Formula	$\text{C}_{13}\text{H}_{18}\text{ClN}_5\text{O}_3\text{Zn}$	$\text{C}_{11}\text{H}_{12}\text{N}_4\text{O}_4\text{Zn}$	$\text{C}_7\text{H}_3\text{N}_3\text{O}_3\text{Zn}$
F_w	393.14	329.62	242.49
Crystal system	Orthorhombic	Orthorhombic	Trigonal
Space group	$Pbca$	$Pbca$	$P3_221$
a (Å)	16.2563(9)	10.189(8)	10.0172(3)
b (Å)	9.870(2)	16.464(14)	10.0172(3)
c (Å)	22.871(2)	17.052(15)	26.2843(8)
α (°)	90	90	90
β (°)	90	90	90
γ (°)	90	90	120
V (Å ³)	3669.7(9)	2861(4)	2284.12(12)
Z	8	8	6
D_c (g·cm ⁻³)	1.423	1.531	1.058
μ (mm ⁻¹)	1.503	1.734	1.602
Observed	3447/3447	3665/3665	6665/2549
R_{int}	0.0321	0.1480	0.0490
GOF on F^2	1.046	1.078	1.013
R^a ($I > 2\sigma(I)$)	0.0753	0.0782	0.0798
wR^b ($I > 2\sigma(I)$)	0.2372	0.2305	0.2161

$$^a R = \sum ||F_o| - |F_c|| / \sum |F_o|, \quad ^b wR = \sum [w(F_o^2 - F_c^2)^2] / \sum [w(F_o^2)^2]^{1/2}$$

Table 2. Selected Bond Lengths (Å) and Angles (°) for Complexes 1~3

Complex 1			
Bond	Dist.	Bond	Dist.
Zn(1)–O(1)	1.942(5)	Zn(1)–N(3)#2	2.038(9)
Zn(1)–N(1)#1	2.029(10)	Zn(1)–Cl(1)	2.226(3)
Angle	(°)	Angle	(°)
O(1)–Zn(1)–N(1)#1	99.6(4)	O(1)–Zn(1)–Cl(1)	118.7(2)
O(1)–Zn(1)–N(3)#2	109.2(4)	N(1)#1–Zn(1)–Cl(1)	111.5(3)
N(1)#1–Zn(1)–N(3)#2	107.5(3)	N(3)#2–Zn(1)–Cl(1)	109.4(2)
Complex 2			
Bond	Dist.	Bond	Dist.
Zn(1)–O(1)	1.972(6)	Zn(1)–N(3)	2.026(6)
Zn(1)–O(3)#3	1.987(6)	Zn(1)–N(1)#4	2.060(6)
Angle	(°)	Angle	(°)
O(1)–Zn(1)–O(3)#3	108.4(3)	O(1)–Zn(1)–N(1)#4	117.5(3)
O(1)–Zn(1)–N(3)	107.8(2)	O(3)#3–Zn(1)–N(1)#4	98.7(2)
O(3)#3–Zn(1)–N(3)	111.8(2)		
Complex 3			
Bond	Dist.	Bond	Dist.
Zn(1)–O(1)#1	1.936(8)	Zn(1)–N(3)#2	1.964(10)
Zn(1)–N(1)	1.933(11)	Zn(1)–O(1W)	1.987(12)
Angle	(°)	Angle	(°)
O(1)#1–Zn(1)–N(1)	118.2(4)	O(1)#1–Zn(1)–O(1W)	100.2(5)
O(1)#1–Zn(1)–N(3)#2	114.4(4)	N(1)–Zn(1)–O(1W)	98.3(5)
N(1)–Zn(1)–N(3)#2	119.5(4)	N(3)#2–Zn(1)–O(1W)	99.7(5)

^a Symmetry transformation used to generate the equivalent atoms for **1**: #1 $-x, -y+1, -z+1$; #2 $x+1/2, -y+3/2, -z+1$; #3 $x-1/2, -y+3/2, -z+1$.

For **2**: #1 $-x+1/2, -y, z-1/2$; #2 $x-1/2, y, -z+1/2$; #3 $-x+1/2, -y, z+1/2$; #4 $x+1/2, y, -z+1/2$.

for **3**: #1 $x-y, -y+1, -z+1/3$; #2 $y, x-1, -z$; #3 $x-y+1, -y+1, -z+1/3$; #4 $y+1, x, -z$.

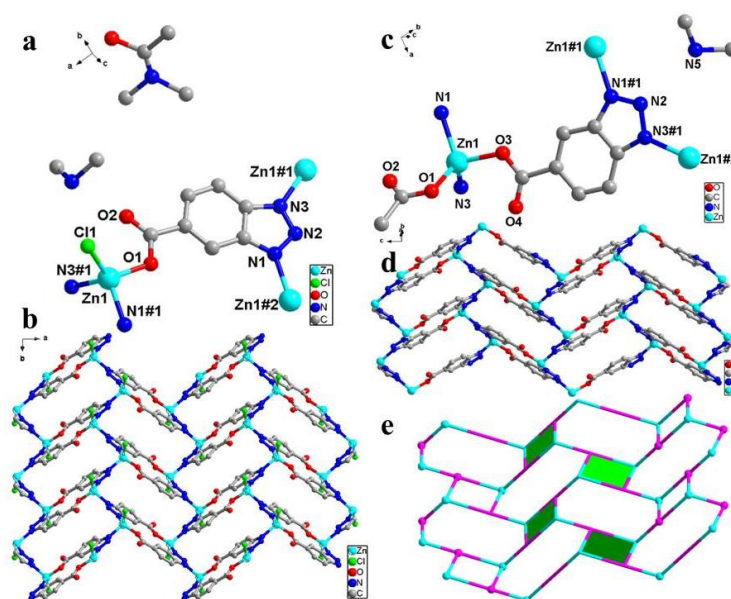


Fig. 1. (a) Asymmetric unit of **1**; (b) Perspective view of the two-dimensional sheet of **1**; (c) Coordination environment of **2**; (d) Two-dimensional layer in **1**; (e) Two-dimensional fes topologic layer in **1** and **2**. Hydrogen atoms are omitted for clarity

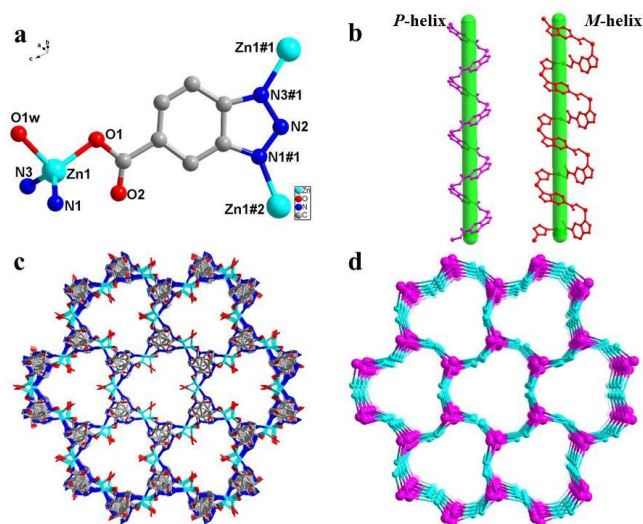


Fig. 2. (a) Coordination environment around the Zn atoms in **3**; (b) Helical chain (*P*- and *M*-helices) in **3**; (c) Perspective view of the three-dimensional framework of **3**; (d) Three-dimensional eta topologic network in **3**. Hydrogen atoms are omitted for clarity

3.2 Powder X-ray diffraction (PXRD)

The purity of **3** can be checked by the powder X-ray diffraction patterns (PXRD). As illustrated in Fig. 3, the curve shape of **3** can exactly match with that of the simulated one, which confirms that complex **3** is very pure. The after-absorbed PXRD patterns are also in good agreement with the as-synthesized samples and the measured single crystals, proving the structure of **3** remains stable in the process of gathering iodine.

3.3 Thermogravimetric analysis (TGA)

The thermogravimetric analysis (TGA) of compound **3** was

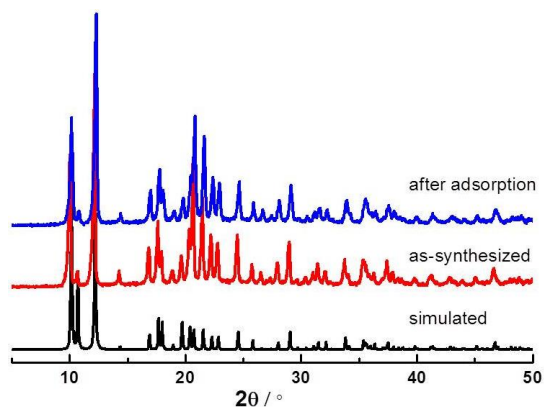


Fig. 3. Characterization of bulk phase of **3** by PXRD

3.4 Absorption performance of I_2

135 mg of prepared samples of **3** was immersed in a cyclohexane solution of I_2 (0.1 mol/L) under room temperature and kept out of light in order to test the ability of I_2 uptake. The color of solution gradually changed from dark red to pale brown, while the color of sample **3** varied from

carried out under N_2 atmosphere with a heating rate of $10\text{ }^\circ\text{C min}^{-1}$ in the range from 30 to 600 $^\circ\text{C}$. As depicted in Fig. 4, the TGA curves reveal that complex **3** exhibited a good thermal stability. The solvents on the sample surface were gradually removed in proceeding from 30 to 120 $^\circ\text{C}$. A slight weight loss of 4.33% was observed between 150 and 300 $^\circ\text{C}$, which could be assigned to the removal of coordinated water molecule (calcd. 6.59%). Over 330 $^\circ\text{C}$, the sharp weight loss up to 550 $^\circ\text{C}$ is due to the decomposition of Pbca organic ligands, accompanying the collapse of the whole framework.

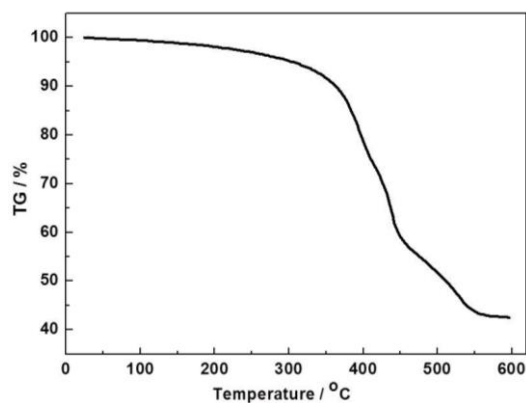


Fig. 4. TGA curves of compound **3**

colorlessness to dark brown (Fig. 5a), which can phenomenally illustrate the adsorption of I_2 . Based on its value-added, the weight of **3** after loading iodine was increased by about 15.6wt%. As shown in Fig. 5b, the compounds after loading iodine may release the absorbents I_2 , resulting in a color variation from colorlessness to pale brown,

which indicates that I_2 sorption is reversible. A little I_2 -loaded sample of **3** was put into 9 mL ethanol. This process can be also proven by the UV-vis spectroscopy at room temperature (Fig. 5c) to further confirm and quantify the above

observation. The absorbance of I_2 extracted into ethanol at 238 nm normally increased over time and the dynamic equilibrium of the release and adsorption of I_2 was reached within 2 hours.

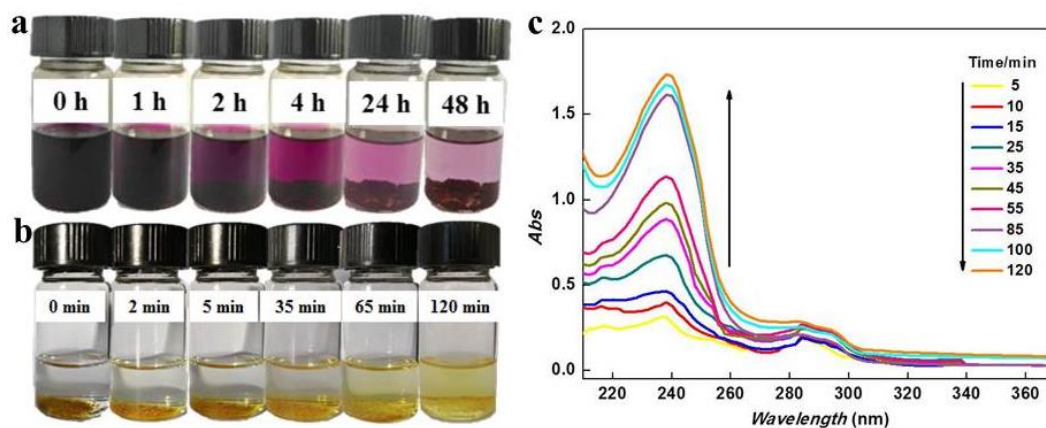


Fig. 5. (a) Photos of the iodine recovery process. (b) Iodine release process of **3** soaked in 9 mL of EtOH. (c) Temporal evolution of UV/vis absorption spectra for the release of I_2 from **3**

4 CONCLUSION

In summary, unusual chiral MOFs have been successfully synthesized by employing achiral multidentate benzotriazole-5-carboxylate acid ligand with N- and O-donors. This success mainly derives from changing synthetic method that urea

derivatives act as structure-directing agent to revolutionize the coordination angle and geometric configuration of inorganic metal ion and organic linker. Interestingly, compound **3** shows excellent performance of enriching iodine. This work could provide a new chance to build chiral framework with achiral organic ligand.

REFERENCES

- (1) Zhang, J. P.; Zhang, Y. B.; Lin, J. B.; Chen, X. M. Metal azolate frameworks: from crystal engineering to functional materials. *Chem. Rev.* **2012**, 112, 1001–1033.
- (2) Pang, J.; Wu, M.; Qin, J. S.; Liu, C.; Lollar, C. T.; Yuan, D.; Hong, M.; Zhou, H. C. Solvent-assisted, thermally triggered structural transformation in flexible mesoporous metal-organic frameworks. *Chem. Mater.* **2019**, 31, 8787–8793.
- (3) Liu, Q.; Song, Y.; Ma, Y.; Zhou, Y.; Cong, H.; Wang, C.; Wu, J.; Hu, G.; O’Keeffe, M.; Deng, H. Mesoporous cages in chemically robust MOFs created by a large number of vertices with reduced connectivity. *J. Am. Chem. Soc.* **2019**, 141, 488–496.
- (4) Su, J.; He, W.; Li, X. M.; Sun, L.; Wang, H. Y.; Lan, Y. Q.; Ding, M.; Zuo, J. L. High electrical conductivity in a 2D MOF with intrinsic superprotonic conduction and interfacial pseudo-capacitance. *Matter* **2020**, 2, 1–12.
- (5) Luo, Y. H.; Dong, L. Z.; Liu, J.; Li, S. L.; Lan, Y. Q. From molecular metal complex to metal-organic framework: the CO_2 reduction photocatalysts with clear and tunable structure. *Coordin. Chem. Rev.* **2019**, 390, 86–126.
- (6) Cui, Y.; Yue, Y.; Qian, G.; Chen, B. Luminescent functional metal-organic frameworks. *Chem. Rev.* **2012**, 112, 1126–1162.
- (7) Kreno, L. E.; Leong, K.; Farha, O. K.; Allendorf, M.; Van Duyne, R. P.; Hupp, J. T. Metal-organic framework materials as chemical sensors. *Chem. Rev.* **2012**, 112, 1105–1125.
- (8) Li, J. R.; Sculley, J.; Zhou, H. C. Metal-organic frameworks for separations. *Chem. Rev.* **2012**, 112, 869–932.
- (9) Horcajada, P.; Gref, R.; Baati, T.; Allan, P. K.; Maurin, G.; Couvreur, P.; Ferey, G.; Morris, R. E.; Serre, C. Metal-organic frameworks in biomedicine. *Chem. Rev.* **2012**, 112, 1232–1268.
- (10) Slater, A. G.; Cooper, A. I. Function-led design of new porous materials. *Science* **2015**, 348, 8075–8085.
- (11) Remya, V. R.; Kurian, M. Synthesis and catalytic applications of metal-organic frameworks: a review on recent literature. *Int. Nano. Lett.* **2019**, 9, 17–29.
- (12) Zhang, Y.; Pang, J.; Li, J.; Yang, X.; Feng, M.; Cai, P.; Zhou, H. C. Visible-light harvesting pyrene-based MOFs as efficient ROS generators. *Chem.*

- Sci.* **2019**, 10, 8455–8460.
- (13) Dong, Z.; Sun, Y.; Chu, J.; Zhang, X.; Deng, H. Multivariate metal-organic frameworks for dialing-in the binding and programming the release of drug molecules. *J. Am. Chem. Soc.* **2017**, 139, 14209–14216.
- (14) Zhao, Y.; Deng, D. S.; Ma, L. F.; Ji, B. M.; Wang, L. Y. A new copper-based metal-organic framework as a promising heterogeneous catalyst for chemo- and regio-selective enamination of β -ketoesters. *Chem. Commun.* **2013**, 49, 10299–10301.
- (15) Wu, Q. Q.; Wen, Y. H. Hydrothermal syntheses, crystal structures and luminescence properties of Zn(II) and Cu(II) complexes based on 2,2'-((sulfonylbis(4,1-phenylene))bis(oxy))diacetic acid. *Chin. J. Struct. Chem.* **2019**, 39, 294–300.
- (16) Jiang, Z. Q.; Li, Y. F.; Zhu, X. J.; Lu, J.; Zhang, L.; Wen, T. Ni(II)-based coordination polymers for efficient electrocatalytic oxygen evolution reaction. *RSC. Adv.* **2018**, 8, 38562–38565.
- (17) Jiang, Z. Q.; Li, Y. F.; Zhu, X. J.; Lu, J.; Wen, T.; Zhang, L. Ni(II)-doped anionic metal-organic framework nanowire arrays for enhancing the oxygen evolution reaction. *Chem. Commun.* **2019**, 55, 4023–4026.
- (18) Jiang, Z. Q.; Chen, X. L.; Lu, J.; Li, Y. F.; Wen, T.; Zhang, L. Ultrathin Ni(II)-based coordination polymer nanosheets as a co-catalyst for promoting photocatalytic H₂-production. *Chem. Commun.* **2019**, 55, 6499–6502.
- (19) Jiang, Z. Q.; Wang, F.; Zhang, J. Rational design of zeolitic tetrazolate frameworks with carboxylate ligands for rapid accumulation of iodine. *Chin. J. Appl. Chem.* **2017**, 34, 1072–1078.
- (20) Seetharaj, R.; Vandana, P. V.; Arya, P.; Mathew, S. Dependence of solvents, pH, molar ratio and temperature in tuning metal organic framework architecture. *Arab. J. Chem.* **2019**, 12, 295–315.
- (21) Kundu, T.; Wahiduzzaman, M.; Shah, B. B.; Maurin, G.; Zhao, D. Solvent-induced control over breathing behavior in flexible metal-organic frameworks for natural-gas delivery. *Angew. Chem. Int. Ed.* **2019**, 58, 8073–8077.
- (22) Li, L. N.; Wang, S. Y.; Chen, T. L.; Sun, Z. H.; Luo, J.; Hong, M. C. Solvent-dependent formation of Cd(II) coordination polymers based on a C₂-symmetric tricarboxylate linker. *Cryst. Growth. Des.* **2012**, 12, 4109–4115.
- (23) Pedireddi, V. R.; Varughese, S. Solvent-dependent coordination polymers: cobalt complexes of 3,5-dinitrobenzoic acid and 3,5-dinitro-4-methylbenzoic acid with 4,4'-bipyridine. *Inorg. Chem.* **2004**, 43, 450–457.
- (24) Köppen, M.; Meyer, V.; Ångström, J.; Inge, A. K.; Stock, N. Solvent-dependent formation of three new bi-metal-organic frameworks using a tetracarboxylic acid. *Cryst. Growth Des.* **2018**, 18, 4060–4067.
- (25) Jiang, Z. Q.; An, Y.; Zhu, X.; Tian, C.; Bai, J.; Li, Y. F. Solvent-dependent synthesis from layer to microporous pillared-layer framework for selective sorption of gas light hydrocarbons. *Z. Anorg. Allg. Chem.* **2015**, 641, 2599–2603.
- (26) Tu, B.; Pang, Q.; Xu, H.; Li, X.; Wang, Y.; Ma, Z.; Weng, L.; Li, Q. Reversible redox activity in multicomponent metal organic frameworks constructed from trinuclear copper pyrazolate building blocks. *J. Am. Chem. Soc.* **2017**, 139, 7998–8007.
- (27) Stock, N.; Biswas, S. Synthesis of metal-organic frameworks (MOFs): routes to various MOF topologies, morphologies, and composites. *Chem. Rev.* **2012**, 112, 933–969.
- (28) Zhang, J.; Chen, S.; Bu, X. Multiple functions of ionic liquids in the synthesis of three-dimensional low-connectivity homochiral and achiral frameworks. *Angew. Chem. Int. Ed.* **2008**, 47, 5434–5437.
- (29) Zhang, J.; Bu, J. T.; Chen, S.; Wu, T.; Zheng, S.; Chen, Y.; Nieto, R. A.; Feng, P.; Bu, X. Urothermal synthesis of crystalline porous materials. *Angew. Chem. Int. Ed.* **2010**, 49, 8876–8879.
- (30) Yoon, M.; Srirambalaji, R.; Kim, K. Homochiral metal-organic frameworks for asymmetric heterogeneous catalysis. *Chem. Rev.* **2012**, 112, 1196–1231.
- (31) Zhang, J.; Bu, X. Chiralization of diamond nets: stretchable helices and chiral and achiral nets with nearly identical unit cells. *Angew. Chem. Int. Ed.* **2007**, 46, 6115–6118.
- (32) Zingiryan, A.; Zhang, J.; Bu, X. Cooperative self-assembly of chiral l-malate and achiral succinate in the formation of a three-dimensional homochiral framework. *Inorg. Chem.* **2008**, 47, 8607–8609.
- (33) Zhang, J.; Chen, S.; Bu, X. Nucleotide-catalyzed conversion of racemic zeolite-type zincophosphate into enantio enriched crystals. *Angew. Chem. Int. Ed.* **2009**, 48, 6049–6051.
- (34) Zhao, X.; Wong, M.; Mao, C.; Trieu, T. X.; Zhang, J.; Feng, P.; Bu, X. Size-selective crystallization of homochiral camphorate metal-organic frameworks for lanthanide separation. *J. Am. Chem. Soc.* **2014**, 136, 12572–12575.
- (35) Jin, J.; Zhao, X.; Feng, P.; Bu, X. A cooperative pillar-template strategy as generalized synthetic method for flexible 3-D homochiral porous

- frameworks. *Angew. Chem. Int. Ed.* **2018**, 57, 3737–3741.
- (36) Zhang, J.; Chen, S.; Wu, T.; Feng, P.; Bu, X. Homochiral crystallization of microporous framework materials from achiral precursors by chiral catalysis. *J. Am. Chem. Soc.* **2008**, 130, 12882–12883.
- (37) Zhang, J.; Chen, S.; Nieto, R. A.; Wu, T.; Feng, P.; Bu, X. A tale of three carboxylates: cooperative asymmetric crystallization of a three-dimensional microporous framework from achiral precursors. *Angew. Chem. Int. Ed.* **2010**, 49, 1267–1270.
- (38) Morris, R. E.; Bu, X. Induction of chiral porous solids containing only achiral building blocks. *Nat. Chem.* **2010**, 2, 353–361.
- (39) Kang, Y.; Chen, S.; Wang, F.; Zhang, J.; Bu, X. Induction in urothermal synthesis of chiral porous materials from achiral precursors. *Chem. Commun.* **2011**, 47, 4950–4952.
- (40) Xiao, J.; Liu, B. Y.; Wei, G.; Huang, X. C. Solvent induced diverse dimensional coordination assemblies of cupric benzotriazole-5-carboxylate: syntheses, crystal structures, and magnetic properties. *Inorg. Chem.* **2011**, 50, 11032–11038.
- (41) Lu, W. G.; Jiang, L.; Lu, T. B. Lanthanide contraction and temperature-dependent structures of lanthanide coordination polymers with imidazole-4,5-dicarboxylate and oxalate. *Cryst. Growth Des.* **2010**, 10, 10, 4310–4318.
- (42) Zhang, W. X.; Xue, W.; Zheng, Y. Z.; Chen, X. M. Two spin-competing manganese(II) coordination polymers exhibiting unusual multi-step magnetization jumps. *Chem. Commun.* **2009**, 45, 3804–3806.
- (43) Guo, Z.; Li, X.; Gao, S.; Li, Y.; Cao, R. A new three-dimensional supramolecular network, $[\text{Cd}(\text{Hbic})_2(\text{H}_2\text{O})]$ (4,4'-bpy) H_2O (H_2bic = 1-H-benzimidazole-5-carboxylic acid; 4,4'-bpy = 4,4'-bipyridine): synthesis, crystal structure and luminescence property. *J. Mol. Struct.* **2007**, 846, 123–127.